Available online at www.sciencedirect.com
ScienceDirect
Coastal Engineering 54 (2007) 279–296
Coastal Engineering
An International Journal for Coastal, Harbour and Offshore Engineers
www.elsevier.com/locate/coastaleng

The morphodynamic modelling of tidal sand waves on the shoreface

P.K. Tonnon [a], L.C. van Rijn [a,b,*], D.J.R. Walstra [a,c]

[a] *Delft Hydraulics, The Netherlands*
[b] *University of Utrecht, The Netherlands*
[c] *Delft University, The Netherlands*

Received 30 January 2006; received in revised form 9 August 2006; accepted 30 August 2006
Available online 13 October 2006

Abstract

An artificial sand wave on the Dutch shoreface of the North Sea has been studied in conditions with relatively strong tidal currents in the range of 0.5 to 1 m/s and sediments in the medium sand size range of 0.2 to 0.5 mm. The sand wave is perpendicular to the tidal current and has a maximum height and length of the order of 5 m and 1 km, respectively. The sand wave is dynamically active and shows migration rates of the order of a few metres per year. A numerical morphodynamic model (DELFT3D model) has been used to simulate the morphological behaviour of the sand wave in the North Sea. This model approach is based on the numerical solution of the three-dimensional shallow water equations in combination with a surface wave propagation model (wind waves) and the advection–diffusion equation for the sediment particles with online bed updating after each time step. The model results show that the sand wave grows in the case of dominant bed-load transport (weak tidal currents; relatively coarse sediment; small roughness height; low waves) and that the sand wave decays in the case of dominant suspended transport (strong currents, relatively fine sediment, large roughness height; storm waves).
© 2006 Elsevier B.V. All rights reserved.

Keywords: Tidal sand waves; Morphological/morphodynamic modelling; Marine sediment transport

1. Introduction

Tidal sand waves with a length scale of about 1 km which are studied in this paper, are common features on the Dutch shoreface of the North Sea (depth range of 10 to 50 m), see Van de Meene (1994) and Hulscher (1996a,b). Generally, these bed features are observed in conditions with relatively strong currents in the range of 0.5 to 1 m/s and sediments in the medium sand size range of 0.2 to 0.5 mm. These sand waves with a maximum height of the order of 5 m are dynamically active and show migration rates of the order of a few metres per year. Generally, the sand wave crests are approximately normal to the tidal current. These sand waves which occur in large fields in the offshore coastal zone offer an easily available source of sand for mining purposes and therefore get increasing attention of coastal managers. In this paper, the behaviour of an artificial sand wave is studied. This artificial sand wave with similar dimensions as natural tidal sand waves was created by dredging sand from the access channel to the port of Rotterdam and dumping this sand on the adjacent shoreface.

Two types of models are generally used to study the behaviour of large-scale bed features: stability models and morphodynamic models, see for overview Hulscher (1996a) and Vittori et al. (2005).

The stability-based models can be used to determine the stability properties of the seabed with respect to arbitrary disturbances. Typically, stability models provide information on the time development of the seabed configuration and can provide the wavelength of the bedforms which tend to appear for given hydrodynamic and morphodynamic conditions. Traditionally, such models have been used to investigate the possible formation of large-scale bedforms, to predict their main geometrical characteristics and to provide a physical explanation of their appearance. Linear stability models yield the bed wave mode (wavelength and crest orientation) which will grow fastest and the growth rate of this mode, indicating the morphological time scale. Non-linear stability models involving the interaction of unstable modes are required to obtain information of the height and shape of the bed wave patterns. Huthnance

* Corresponding author. Delft Hydraulics, The Netherlands.
E-mail address: leo.vanrijn@wldelft.nl (L.C. van Rijn).

0378-3839/$ - see front matter © 2006 Elsevier B.V. All rights reserved.
doi:10.1016/j.coastaleng.2006.08.005

(1982) was the first to develop a simplified linear stability model to disclose the mechanism originating open shelf sand banks. According to Huthnance (1982), sand banks are generated by the deflection of a tide-driven current crossing a bank. The current deflects towards the bank crest due to an increased effect of bottom friction with a decreasing water depth. The along-ridge velocity decreases due to the increase of bottom friction and the cross-bank velocity increases to satisfy continuity. The net current and transport on the flanks are thus directed towards the crest of the bank both for the flood and the ebb phases of the tide. Huthnance (1982) used a simple flow model (a simplified version of depth-averaged shallow water equations), a power–law relationship to evaluate sediment transport rate and the conservation of sediment. The morphological time scale was assumed to be much longer than the hydrodynamic time scale and the hydrodynamic problem was thus decoupled from that of the bottom development. The basic state was a flat bed configuration subject to a simple periodic flow. Later, a more refined model was formulated by Hulscher et al. (1993). The fluid motion is still described by the depth-averaged shallow water equations but in complete form. Recently, Roos (2004) and Roos et al. (2004) extended the linear stability analysis into the finite amplitude regime using a non-linear process-based model. The main shortcoming of models based on the depth-integrated shallow water equations is that they can only predict modes corresponding to sand banks but they cannot simultaneously predict modes corresponding to sand waves. In fact, the formation of sand waves is related to the presence of steady recirculating cells in the vertical direction generated by the interaction of the oscillatory tidal flow with the bottom waviness. Since, the description of the 3D recirculating cells cannot be obtained by means of the depth-averaged shallow water equations, Hulscher (1996b) has presented a linear three-dimensional stability model based on a constant viscosity and partial slip at the bottom. Depending on the values of the model parameters, a flat bottom turns out to be either stable against all possible regular perturbations or unstable. In the latter case a wavy bottom pattern develops. Three different types of the initially most unstable modes can be identified: tidal sand banks, tidal sand waves normal or oblique to the main tidal current and tide-parallel sand waves. Hulsher (1996b) has shown that tidal sand waves are generated by the interaction of the basic current and the perturbated tidal components in the water column. Vertical effects (modification of the velocity profiles) have to be included to explain the generation of sand waves due to tide–topography interactions, which cannot be described by a depth-averaged approach. According to Hulscher (1996b), relatively large flow resistance leads to sand waves with their crest normal to the main tidal current direction. Less flow resistance leads to the rotation of the sand wave crests due to veering of the currents in the vertical direction. At very low flow resistance the crests become nearly parallel to the main current direction. The model by Hulscher (1996b) has been extended by Besio et al. (2003) who, solving Reynolds equations by means of a method taking into account the cascade process which gives rise to a large number of time harmonic components, obtained results which compare fairly good with field observations. Further contributions to the study of sand waves are those by Nemeth et al. (2002) and Besio et al. (2004a) who introduced the effect of the residual current and the tide asymmetry respectively in the models by Hulscher (1996b) and Besio et. al. (2003). A more refined model describing the generation and evolution of both tidal sand banks and sand waves from bottom perturbations of a flat seabed subject to the action of tidal currents has been developed by Besio et al. (2004b). A horizontally two-dimensional basic flow forced by a tidal wave is considered and Coriolis effects are taken into account. The basic flow is completely resolved in the vertical direction from the free surface down to the seabed where the no-slip condition is forced. The sediment is supposed to move as both bed load and suspended load.

A basic restriction of these types of stability models is that the sand wave shape is sinusoidal, the sand wave height is relatively small and strictly infinitesimal. Generally, the bed-load and suspended-load transports are taken into account using rather simple transport equations; the entrainment and transportation of the suspended sediments (lag effects) requiring the application of the advection–diffusion equation for the sediment concentration usually is neglected. The same holds for the effect of the orbital wave motion on the suspended sediment transport. Usually, the effect of short surface waves on the sediment transport process is neglected in stability model approaches.

In this paper, the other available model approach is used: morphodynamic modelling, which is based on the application of a numerical morphodynamic model (DELFT3D model). This model approach is based on the numerical solution of the three-dimensional shallow water equations in combination with a surface wave propagation model (wind waves) and the advection–diffusion equation (to include lag effects) for the sediment particles with online bed updating after each time step. This model includes bed-load and suspended-load transports and a bed roughness predictor depending on the hydrodynamic and sediment conditions (Van Rijn et al., 2004; Van Rijn, 2006a, submitted for publication). A major advantage of this approach is that many effects acting on uniform, cohesionless sediment particles moving along tidal sand waves are included, which however requires a relatively large computational effort restricting 3D model application to a time span of the order of 10 to 20 years at present state of computer technology. Certain mechanisms such as cohesive effects and hiding/exposure effects of heterogeneous sediments are not considered. Finally, it is noted that numerical morphodynamic models are very well suited to simulate the transient behaviour of sand waves of arbitrary shape on the medium term time scale of 10 to 20 years in contrast to stability-based models which are more aimed at the long-term behaviour of idealized wave shapes for strongly schematised forcing conditions.

To evaluate the ability of this numerical 3D model with respect to the morphological behaviour of tidal sand waves, an artificial sand wave near Hoek van Holland (close to Rotterdam harbour, The Netherlands) has been studied in great detail.

This paper presents the data of the sand wave studied, the description of the model set-up, a detailed sensitivity analysis

using an idealized sand wave to gain insight in the physical processes of the flow and transport at the sand wave and to study the effect of tides, waves and basic model settings on the morphological development of an idealized sand wave. Finally, the numerical simulation results of the artificial sand wave in the North Sea on a time scale of 15 years are presented.

2. Artificial sand wave in North Sea

From 1982 to 1986 an artificial sand wave was created by dumping approximately 3.5 million m^3 of sand (Van Woudenberg, 1996) which was dredged from the shipping channel to Rotterdam harbour, onto the shoreface (depths between −15

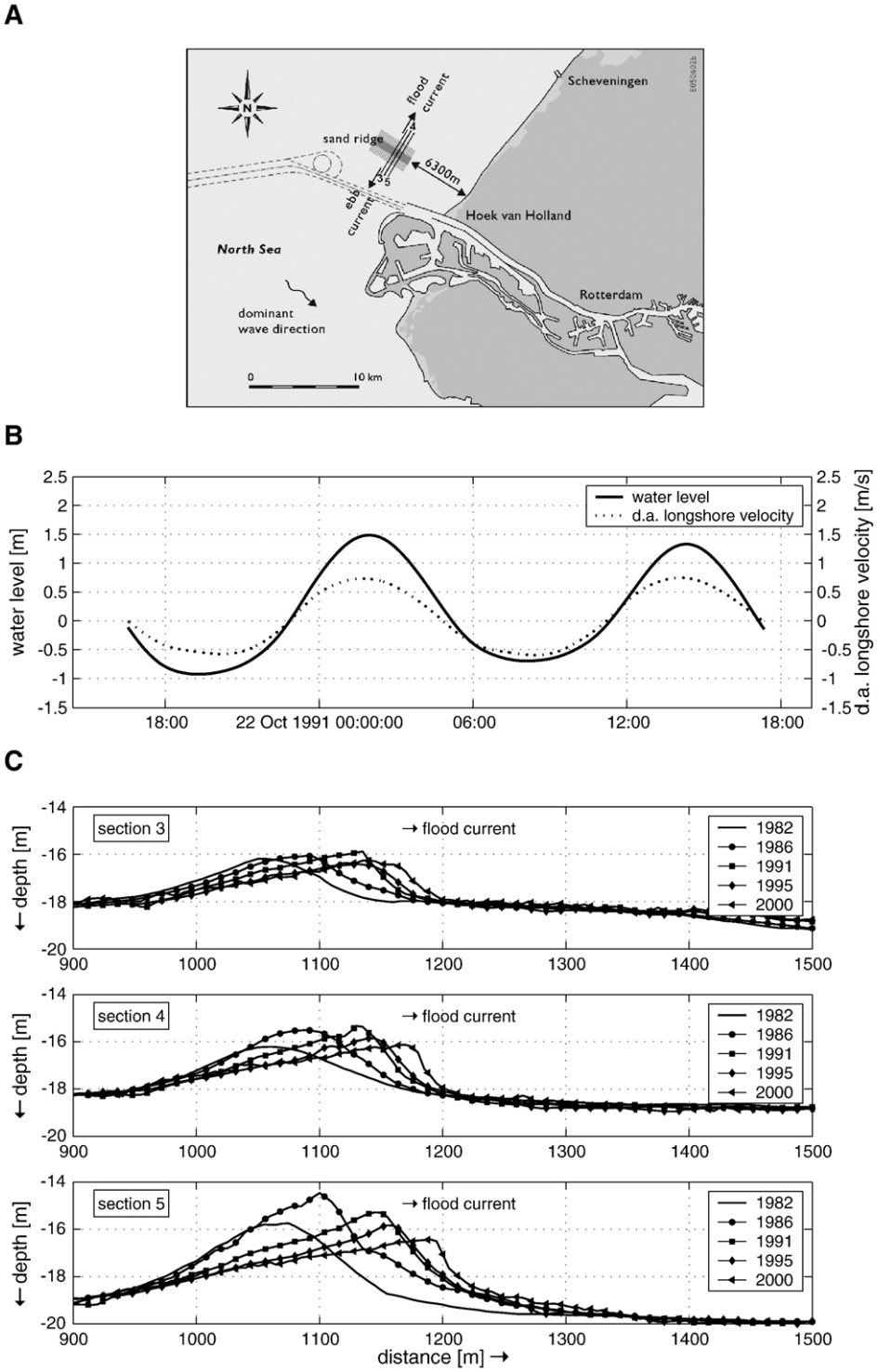

Fig. 1. A: Plan view location of the artificial sand wave Hoek van Holland; cross-section 3 is landward, cross-section 5 is seaward. B: Horizontal and vertical tide at a depth of 18 m at location Hoek van Holland. C: Measured bed levels for cross-sections 3, 4 and 5.

and −23 m to MSL) at the location Hoek van Holland immediately north of the approach channel to the port of Rotterdam, see Fig. 1A. The composition of dumped sand is similar to that of ambient sediment. The sand wave is more or less perpendicular to the coast, the sand wave dimensions just after creation were: length of about 3600 m; toe width between 250 and 370 m; height between 1.3 and 4 m; slopes between 1:50 and 1:100 on the south flank and between 1:20 and 1:50 on the north flank; D_{50} between 0.15 and 0.45 mm. The landward end of the sand wave is about 6300 m from the shoreline. The tidal flow with peak flood velocities of about 0.7 m/s to the north–east and peak ebb velocities of about 0.6 m/s to the south–west is parallel to the coast and thus normal to the sand wave crest.

Fig. 1B shows the computed horizontal and vertical tide at a depth of 18 m at location Hoek van Holland, two and a half days before springtide. The daily inequality with water levels varying between −1 m and 1.5 m is shown and it can be seen that there is only a very small phase difference between the horizontal and vertical tide.

Between 1982 and 2000 bathymetric surveys of the sand wave were carried out by Directorate North Sea (DNZ) of Rijkswaterstaat. Data collection before 1991 was carried out using the single-beam method, while data collection after 1991 was carried out using the more accurate multi-beam method. The vertical accuracy of the soundings is of the order of 0.1 to 0.2 m; the horizontal accuracy is of the order of 1 to 5 m.

Fig. 1C shows measured bed levels for cross-sections 3, 4 and 5 (see Fig. 1A) for the period 1982–2000. Between 1982 and 1986 the sand dumpings contributed to the vertical growth of the sand wave. Measurements for the period 1986–2000 show a clear reduction in sand wave height and a net migration of the crest in northern (flood) direction. Since the migration rate decreases with depth (18 m in cross-section 4 to about 25 m in cross-section 9), the sand wave shows a slight rotation with respect to the original axis. The base of the sand wave hardly changes over a period of 15 years. Hence, the shape of the sand wave is modified slightly (more asymmetric). The average rate of migration of the crest in the flood direction to the north–east is about 5.5 m per year and the average decrease in height is about 0.1 m per year (period 1982 to 2000).

3. Model approach, set-up and calibration

3.1. Models

In this paper the DELFT3D modelling system developed by WL|Delft Hydraulics has been used to study the morphological development of a sand wave perpendicular to the main tidal direction covering a period of 5 to 15 years and focussing on cross-section 4 of the sand wave (Fig. 1C). DELFT3D can simulate flows, waves, sediment transports and morphological developments and consists of several modules (see Lesser et al. 2004). Various turbulence models (algebraic, k–L and k–ϵ models) are available to be selected by the user. A brief description of the WAVE, FLOW and morphological SEDIMENT-ONLINE submodels is given herein. The evolution of wind-generated waves can be simulated using the DELFT3D-WAVE module, which is based on either HISWA or SWAN models; a spatially constant wave height can also be used (for the latter no Wave model is required and is directly prescribed in the Flow module). The wave parameters calculated in DELFT3D-WAVE module are used as input for the DELFT3D-FLOW module, to compute wave-driven currents, enhanced turbulence, bed-shear stress and sediment stirring by wave breaking. The DELFT3D-FLOW module is a hydrodynamic simulation program, which calculates non-steady flow and transport phenomena resulting from tidal, wind, wave and/or meteorological forcing on a curvilinear, boundary fitted grid. The numerical system solves the unsteady shallow water equations in two or three dimensions. The DELFT3D model can be operated in rectangular or in curvilinear grid mode, in transect mode or in area mode and in single layer (depth-averaged; 1DH or 2DH) or multi-layer (2DV or 3D) mode with an online coupling between hydrodynamic and transport/bottom modules which implies that the flow, transport and bottom updating are now merged into the SEDIMENT-ONLINE model, only the wave model is executed separately (data communication between online model and wave model). The SEDIMENT-ONLINE module enables the simultaneous computation of flows and transports and the associated bed updating at every flow time step. The bed evolution can be upscaled (accelerated) after each time step by means of a so-called morphological upscaling factor, MORFAC (e.g. with MORFAC = 100, a morphological prediction based on a tidal cycle of 12.5 h would represent 12.5 × 100 h = 52 days). The morphological upscaling factor has to be prescribed by the user and depends on the dynamic response of the area of interest; dynamic areas require a lower MORFAC value whereas for more stable environments the MORFAC can be increased (typical range is between 10 and 1000 for dynamic and stable areas respectively).

The SEDIMENT-ONLINE model includes a bed roughness predictor, which represents the presence of grain and bedform roughness based on hydrodynamic and sediment conditions (Van Rijn et al., 2004; Van Rijn, 2006a, submitted for publication). This predictor specifies a bed roughness value (k_s) accounting for the presence of small-scale current-related and wave-related ripples, current-related megaripples in the lower regime and flat bed in the upper regime.

The suspended sediment transport in the 3D model is based on the numerical solution of the advection–diffusion equation, as follows:

$$\frac{\partial[hC]}{\partial t}+\frac{\partial[hUC]}{\partial x}+\frac{\partial[hVC]}{\partial y}+\frac{\partial((\omega\text{-}w_s)C)}{\partial \sigma} = h\left[\frac{\partial}{\partial x}\left(\varepsilon_{s,x}\frac{\partial C}{\partial x}\right)+\frac{\partial}{\partial y}\left(\varepsilon_{s,y}\frac{\partial C}{\partial y}\right)\right]+\frac{1}{h}\frac{\partial}{\partial \sigma}\left[\varepsilon_{s,z}\frac{\partial C}{\partial \sigma}\right]+hS \quad (1)$$

with: U,V = fluid velocities in x, y-directions, ω = vertical fluid velocity relative to the moving vertical coordinate (σ)-plane, h = flow depth, C = concentration, w_s = settling velocity of suspended sediment, S = source and sink terms and ϵ_s =

sediment diffusivity coefficients in x, y, z-directions. The sediment transport module was recently updated based on the TRANSPOR2004 sand transport formulations (Van Rijn et al., 2004; Van Rijn 2006a, submitted for publication).

3.2. Sub-grid model for reference concentration of suspended transport

The computation of the suspended sediment transport according to Eq. (1) is based on the concept of a reference concentration (bed boundary condition) very close to the bed (at level $z=a$), as proposed by Van Rijn (1984, 1993, 2006a, submitted for publication). To extrapolate or interpolate this value to the first grid point of the DELFT3D model, a sub-grid model is used which accounts for hindered settling and turbulence damping effects using a refined sub-grid with 20 grid points in the lowest layer of the model. This is effectuated by modifying the source and sink terms in the lowest layer each half time step.

3.3. Sediment transport and bed level evolution

The bed level evolution is based on the sediment continuity equation (mass balance), which reads as:

$$\frac{\partial z_b}{\partial t}+\frac{\partial\left(S_{b,x}+S_{s,c,x}+S_{s,w,x}\right)}{\partial x}+\frac{\partial\left(S_{b,y}+S_{s,c,y}+S_{s,w,y}\right)}{\partial y}=0 \tag{2}$$

Eq. (2) can also be expressed as:

$$\frac{\partial z_b}{\partial t}+\frac{\partial\left(S_{b,x}+S_{s,w,x}\right)}{\partial x}+\frac{\partial\left(S_{b,y}+S_{s,w,y}\right)}{\partial y}+\left(\varepsilon_{s,z}\frac{\partial C}{\partial \sigma}\text{-}(\omega\text{-}w_s)C\right)_{near\text{-}bed}=0 \tag{3}$$

with:

- $S_{b,x,y}$ bed-load transport in x, y-direction (U,V-velocity direction),
- $S_{s,c,x,y}$ current-related suspended-load transport in x, y-direction,
- $S_{s,w,x,y}$ wave-related suspended-load transport in x, y-direction,
- $\epsilon_{s,z}$ mixing coefficient at lowest grid point; w_s=settling velocity, C=concentration.

In the case of a sloping bed (longitudinal and transverse slopes) the bed-load transport vector (S_b) has to be modified to include the slope effects, as follows: (1) modification of the bed-load transport in s-direction (in direction of bed-load transport vector) based on the Bagnold approach (Bagnold, 1956); and (2) addition of slope-related bed-load transport vector ($q_{b,n}$) in n-direction (normal to s-direction) based on the Ikeda approach (Ikeda, 1982). In the present study the Bagnold factor acting on the bed-load particles at sloping beds is of most interest. The Bagnold factor reads as: $\alpha_s=\tan\phi/[\cos\beta(\tan\phi-\tan\beta)]$ with: β = longitudinal slope and ϕ = angle of internal fraction (angle of repose). This factor reduces the bed-load transport in upsloping flows and increases the bed-load transport in downsloping flows.

The last term of Eq. (3) represents the vertical sedimentation and erosion terms at the upper interface of the lowest grid cell. The bed-load transport contributions are based on a quasi-steady intra-wave approach, which implies that the bed-load transport is assumed to respond almost instantaneously to orbital velocities within the wave cycle including the prevailing current velocity. Similarly, the wave-related suspended-load transport contribution ($S_{s,w}$) is assumed to respond almost instantaneously to the orbital velocities. This latter transport contribution can be formulated in terms of time-averaged (over the wave period) parameters resulting in a relatively simple transport expression.

The current-related suspended-load transport is based on the variation of the suspended sand concentration field due to the effects of currents and waves. Using a 2DH approach (1 layer), the sand concentration field is described in terms of the depth-averaged equilibrium sand concentration derived from equilibrium transport formulations and an exponential adjustment factor based on the (numerical) method of Galappatti (1983). Using a 3D approach (multiple layers), the sand concentration field is based on the numerical solution of the 3D advection–diffusion equation (Eq. (1)). In the latter approach, the current-related suspended transport components are defined as:

$$S_{s,c,x}=\int_a^h\left(uc\text{-}\varepsilon_{s,z}\frac{\partial c}{\partial x}\right)dz;\quad S_{s,c,y}=\int_a^h\left(vc\text{-}\varepsilon_{s,z}\frac{\partial c}{\partial y}\right)dz \tag{4}$$

All the transport formulations contain calibration factors (input values): f_{BED} (on the bed-load transport), f_{SUS} (on the reference concentration) and f_{SUSW} (on the wave-related suspended transport). These factors are applied as constants in the spatial and temporal domain. Default values are 1, which implies that the formulations represent the physics of the sand transport process perfectly. Using these factors, the user of the model can up or downscale the transport rates to calibrate the model if transport data and/or bathymetry data are available. As stated before, the bed evolution can be upscaled (accelerated) after each time step by means of a so-called morphological upscaling factor (MORFAC).

3.4. Model set-up and calibration

Since, the tidal sand wave at the location Hoek van Holland is situated almost fully perpendicular to the tidal velocities (no oblique flow), most model runs were executed in 2-dimensional vertical mode (2DV), assuming uniform conditions in lateral direction along the sand wave crest. Some runs have been made in 3D mode considering the entire width of the sand wave (normal to the coast), yielding similar results at cross-section 4 as the runs in 2DV-mode and are, therefore, not discussed in this paper.

The 2-dimensional vertical model (2DV) along sand wave section 4 (see Fig. 1A) has been set up to compute the residual sand transport over a full neap–spring tidal cycle. The 2DV

model application is based on the large-scale DELFT Holland Coastal Zone model (Roelvink et al., 2001), referred to as the HCZ model. A small, detailed grid based on the 1986 bathymetry was constructed by locally refining the HCZ grid to accurately represent the sand wave profile. A vertical grid of 20 layers with logarithmic layer distribution was used. Boundary conditions were derived from the HCZ model. Current velocities are specified at the southern boundary of the model and water levels are specified at the northern boundary. A computational time step of 15 s was used. Other model parameters are as follows. Wind: a constant representative wind speed of 7 m/s from 240°N (Southwest) was applied. Waves: the single representative wave condition from Walstra et al. (1997) was used yielding a significant wave height of 2.25 m, period of 6.6 s, direction of 315°N. Sediment: D_{50} equal to 0.3 mm, D_{90} of 0.6 mm. Bed roughness: the bed roughness predictor implemented in DELFT3D has been used to compute the effective bed roughness height of Nikuradse (k_s) as function of hydrodynamic and sediment parameters (Van Rijn et al., 2004) resulting in k_s-values in the range of 0.02 to 0.2 m. The Coriolis acceleration is set up for 52°N; acceleration of gravity set to 9.81 m/s^2; air density set to 1 kg/m^3; water density set to 1025 kg/m^3; salinity set to 31 ppt and water temperature set to 15 °C.

The 2-dimensional vertical (2DV) longshore model of sand wave section 4 (see Fig. 1A) was calibrated to give a northward residual transport of about 18 m^3/m/year, based on earlier estimations of the net annual transport rates at depths of −20 and −8 m NAP (Dutch Ordnance Datum) in that region of the Dutch shoreface (Van Rijn, 1997). It was found that a multiplication factor on both bed-load and suspended-load transport rates of 0.4 resulted in a northward residual transport of 18 m^3/m/year. This factor on bed-load and suspended-load transports of 0.4 is applied in all computations hereafter.

4. Model runs for idealized sand wave schematisation

4.1. Idealized sand wave schematisation

A longshore 2DV model (assuming no flow normal to the cross-section) was set-up to gain insight in the physical processes of an idealized sand wave and to study the effect of tides, waves and basic model settings on the morphological development over 5 years. The 2DV approach is based on the assumption of uniform flow in lateral direction (no flow normal to the plane of the cross-section). This assumption is considered to be valid for the field case of the artificial sand wave (at the Hoek van Holland site), which is perpendicular to the tidal velocity field (no oblique flow). The idealized sand wave consists of a symmetrical sand wave (sediment size of D_{50}=0.3 mm; D_{90}=0.6 mm, see Table 1and 2) which is a schematic representation of the sand wave characteristics of section 4 (see Fig. 1C) in 1991, i.e. a mean depth outside the sand wave of −17.8 m to MSL, a sand wave height of about 3 m and a sand wave width of about 400 m. The sand wave volume is 530 m^3/m. The tidal flow is represented by a sinusoidal function ($U=U_0+U_1\cos(\omega t)$; $h=h_0+\zeta\cos(\omega t)$) with and without a net current (U_0), thus representing a propagating tidal wave as present in the Dutch coastal zone (U_0 = net tidal current, U_1 = velocity amplitude, ζ = water level amplitude, h_0 = mean water depth, $\omega=2\pi/T$=wave number, T = tidal period). The small phase difference between horizontal and vertical tide was neglected. A scaling factor of 0.4 on both the bed-load and suspended-load transports was used. The model was run in depth-averaged mode (1DH) and in 2-dimensional vertical mode (2DV) with 20 layers. Most of the runs in 2DV mode. Harmonic water levels are prescribed at the northern boundary; harmonic velocities (logarithmic profiles) at the southern boundary. The western and eastern boundaries are closed boundaries. Equilibrium concentration profiles are prescribed at both the northern and southern boundaries. The perfect representation of time variation of the tidal current based on the unsteady flow equations is not strictly required. A series of combinations of steady flow situations (with constant water level and discharge) would give the same overall results.

Table 1
Process and model parameters

Process and model parameters	Variation
Model approach	1DH (1 layer) / 2DV (20 layers)
Median sediment diameter (D_{50})	D_{50} = 0.2, 0.25, 0.3 and 0.35 mm
Tides without net current	Velocity amplitudes (U_1) of 0.5, 0.75 and 1 m/s
Bed roughness schematisation	Variable, constant (C = 65, 75 and 85 m$^{1/2}$/s)
Turbulence model	Algebraic, k–L and k–epsilon (ϵ)
Waves without and with net current	H_s = 0, 2 and 3 m, net current of 0 and 0.1 m/s; wave direction is 315° to North
Longitudinal bed-slope factor	ALFABS = 1, 3 and 5

4.2. Basic processes

An essential feature to be modelled is the adjustment of the velocity profiles when the flow passes the sand wave. In unidirectional flow the velocity profiles have a different shape at both sides of the crest of the sand wave; the velocity profiles upstream of the sand wave crest are characterized by increasing velocities in the near-bed zone (bulgy shape due to decreasing water depth), while downstream of the crest the velocity profiles are characterized by reduced velocities in the near-bed zone (dipped shape due to increasing water depth and deceleration processes), see Fig. 2.

In the case of tidal flow, the direction of the flow changes with the turning of the tide which has its consequences on the time-averaged (residual) velocity profiles at both sides of the sand wave. At maximum flood and maximum ebb flow, the velocity profiles show increased velocities at the upstream flank and reduced velocities at the downstream flank. As the flow during flood and ebb is in opposite direction, the upstream and downstream locations are at opposite sides of the sand waves crest; the bulgy velocity profiles change to dipped velocity profiles when the flow reverses. The time-averaged (residual) velocity profiles at both flanks therefore show a vertical distribution as given in Fig. 3; at both flanks the time-averaged

Table 2
Sediment characteristics and model results for idealized sand wave

Run	D_{10} [mm]	D_{50} [mm]	D_{90} [mm]	Net annual bed-load transport [m^3/m /year]	Net annual suspended-Load transport [m^3/m /year]	Net annual total transport [m^3/m /year]	Sand wave volume [m^3/m]
1	0.15	0.2	0.4	21	110	131	470
2	0.17	0.25	0.5	32	42	74	525
3	0.2	0.3	0.6	28	24	52	530
4	0.23	0.35	0.7	24	19	43	535

(residual) near-bed velocities are directed toward the sand wave crest. This can be interpreted as a vertical circulation cell.

This mechanism results in vertical growth of the sand wave when bed-load transport is dominant; the particles remain in the crest region of the sand wave and are transported towards the sand wave crest. When suspended-load transport higher in the vertical is dominant, the sediment particles can be transported beyond the crest region towards the sides of the sand wave resulting in flattening of the sand wave.

Another important effect during tidal flow is the continuously changing water depth. The tidal range with decreasing water depths during ebb and increasing water depths during flood affects velocities, transport rates and morphology. The bed-shear stress depends on the water depth; the bed-shear stress will be larger during ebb flow with shallower water depth at the same depth-averaged velocity. Assuming equilibrium flow with approximately logarithmic velocity profiles at the upstream flank of the sand wave, the bed-shear stress can be estimated by:

$$\vec{\tau}_b = \frac{g\rho \vec{U}|\vec{U}|}{C^2} \text{ and } C = 18\log\left(\frac{12h}{k_s}\right) \quad (5a, b)$$

with: τ_b = bed-shear stress [N/m^2]; g = gravitational acceleration [m/s^2]; ρ = water density [kg/m^3]; U = velocity [m/s]; C = Chézy coefficient [$m^{1/2}$/s]; k_s = equivalent roughness of Nikuradse [m].

The effect of waves on the bed-shear stress and sand transport also depends on the water depth. Waves in shallower water depth intensify the stirring action of the oscillatory fluid motion in the near-bed region which leads to larger sediment concentrations and larger transports; with shallower water the effect will be greater and transports will be larger. Thus, assuming equal depth-averaged ebb velocities and flood velocities, the transport rates in ebb direction (at upstream flank) are larger than the transport rates in flood direction due to both larger bed-shear stresses and increased wave action during ebb.

4.3. Model parameters

First, the sensitivity of the model results to various values of the horizontal grid size is shown for the case with a net current of 0.1 m/s (asymmetrical tide; peak flood velocity to north of 0.85 m/s; peak ebb velocity to south of 0.65 m/s) with waves. The sand wave migrates in the dominant flood direction to the north. The model results are weakly sensitive (quantitatively, but not qualitatively) to the horizontal grid size applied due to numerical diffusion; the morphological development of the sand wave converges for relatively small grid sizes of 2.5 and 5 m and a time step up of 15 s, see Fig. 4. The model runs hereafter are applied on a horizontal grid with size of 10 m, a time step of 15 s and a morphological acceleration factor (MORFAC) of 182.5 to reduce on computational time. It was found that MORFAC values up to 500 may be used to speed up morphological changes without affecting hydrodynamics and morphodynamics in the offshore zone with depths larger than about 15 m.

Fig. 5 shows the five-year bottom profile development for simulations using the algebraic, k–L and k–epsilon (ϵ) turbulence models. The algebraic turbulence model is based on the parabolic–linear sediment mixing of Van Rijn (1993). The sand wave migrates in the direction of the dominant flood current to the north (on right side of the sand wave). It can be seen that the morphological development of the sand wave is affected by the choice of the turbulence model, which affects the distribution of sediment over the water column and hence the proportion of bed-load and suspended transports and thus the growth or damping of the sand wave. Furthermore it is found that the north flank of the sand wave becomes somewhat steeper using the algebraic turbulence model than using the k–L or k–ϵ turbulence model. Using the k–ϵ turbulence model, a dip develops at the north toe of the sand wave due to enhanced bed-shear stresses at that location. The dip development at the north toe based on the k–ϵ model is not fully understood. It may indicate how the sand wave instability gradually spreads out to

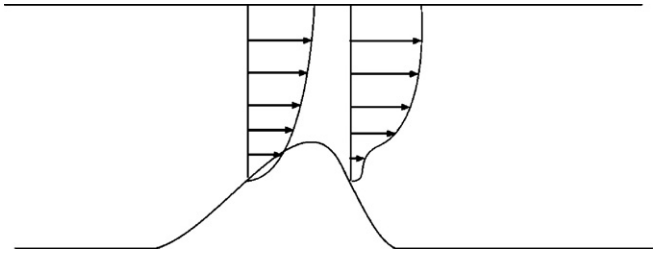

Fig. 2. Velocity profiles over sand wave.

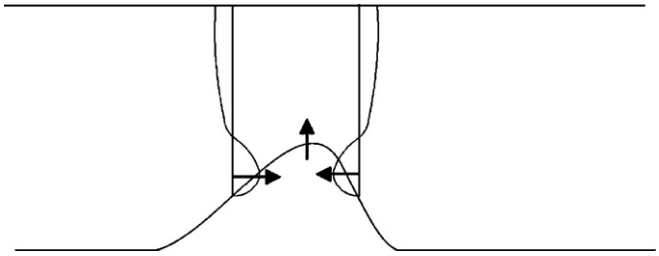

Fig. 3. Time-averaged (residual) velocity profiles at flanks of the sand wave.

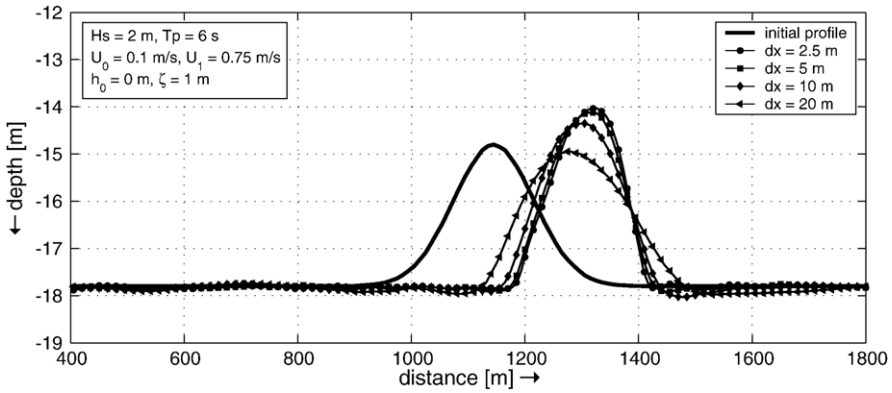

Fig. 4. Five-year bottom profile development in case of net current with waves based on horizontal grid sizes of 20, 10, 5, and 2.50 m (south on left side and north on the right side of sand wave).

the area next to the sand wave to create adjacent troughs, as found by Roos (2004) and Roos et al. (2004). Given this uncertainty and the fact that this phenomenon has not been observed in the field case, the algebraic turbulence model has been used as the standard model in this study.

4.4. Model results for idealized sand wave

A series of model runs varying process and model parameters has been performed to identify the most essential parameters influencing the sand wave morphology. The process and model parameters are given in Table 1.

4.4.1. Model approach; effect of vertical flow structure

Fig. 6 shows the five-year bottom profile development for a symmetrical tide (no net current; peak flood and ebb velocity of 0.75 m/s) without waves based on simulations in 1DH mode and 2DV mode. For both simulations the sand wave migrates in ebb direction due to smaller water depth during ebb. This results in a relative enhanced stirring of sediment and thereby increasing the transport capacity during the ebb phase. The sand wave increases in height using the 2DV model approach, because a vertical circulation cell is generated by the model causing a net flow towards to the crest resulting in vertical wave growth in this case with relatively coarse sediment of 0.3 mm (base case run 3; dominant bed-load transport; see Table 2). Since vertical circulation cells can not be simulated by the 1DH model, vertical growth is absent. The wave crest shows a slight decay in the latter case due to slope effects on bed-load transport. The sand volume of the sand wave based on 1DH and 2DV model results is about the same (530 $m^3/m \pm 1\%$).

The left plot of Fig. 7A shows the absolute values of the bed-shear stress at maximum flood and maximum ebb flow for the 2DV simulation without a net current and no waves. It can be seen that during ebb the bed-shear stress at the sand wave is higher than during flood due to the reduced water depth during ebb. This results in larger transport rates during ebb than during flood and a migration in ebb direction, as shown in the right plot of Fig. 7A.

Fig. 7B shows tide-averaged velocity profiles at six locations for the 2DV simulation without a net current and no waves. It can be seen that tide-averaged near-bed velocities at both flanks of the sand wave are directed toward the sand wave crest due to the deformation of the velocity profiles over the sand wave.

This mechanism results in vertical growth of the sand wave when bed-load transport is dominant; the particles remain in the crest region of the sand wave and are transported towards the sand wave crest. When suspended-load transport higher in the

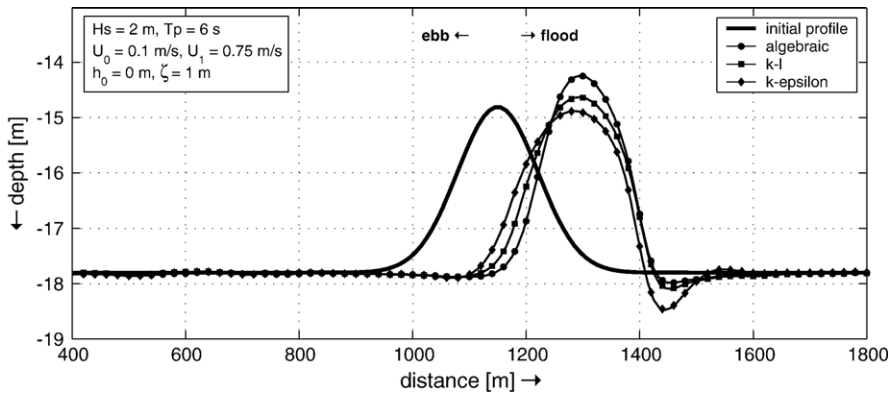

Fig. 5. Five-year bottom profile development in case of a net current of 0.1 m/s with waves based on algebraic, k–L and k–epsilon (ϵ) turbulence model (south on left side and north on right side).

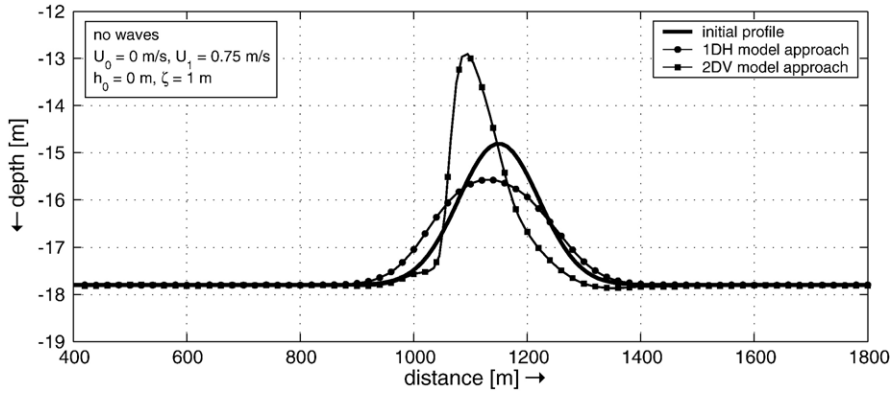

Fig. 6. Five-year bottom profile development using 1DH and 2DV model approach without waves.

vertical is dominant, the sediment particles can be transported beyond the crest region towards the sides of the sand wave resulting in flattening of the sand wave.

4.4.2. Effect of median sediment diameter

Fig. 8 shows the five-year bottom profile development from simulations using a median sediment diameter (D_{50}) of 0.2, 0.25, 0.3 and 0.35 mm for a tide with velocity amplitudes of 0.75 m/s and a net current of 0.1 m/s in flood direction with waves (H_s=2 m). The sediment characteristics (D_{10}, D_{50} and D_{90}) used are given in Table 2. This range of values is similar to the range in sediment diameters found on the sand wave at section 4 (Fig. 1A). The sediment diameter affects the relative contributions of bed-load and suspended-load transports and the overall net annual transport (see Table 2). The net annual bed-load transport varies in the range of 20 to 30 m^3/m/s; the net annual suspended transport varies in the range of 20 to 110 m^3/m/s and decreases with increasing grain diameter. The bed-load transport is only weakly affected by the grain diameter. The variation range of the bed-load transport of the runs involved (Table 2) is almost fully related to the variable bed roughness applied affecting near-bed velocities and hence bed-shear stresses in combined wave–current conditions (see Van Rijn, Part I, submitted for publication). A smaller sediment diameter of 0.25 mm yields a larger net annual total transport rate (about 50%) compared to the case with D_{50}=0.3 mm. The results show that the sand wave increases in height using a median sediment diameter of 0.3 and 0.35 mm (dominant bed load) and decreases

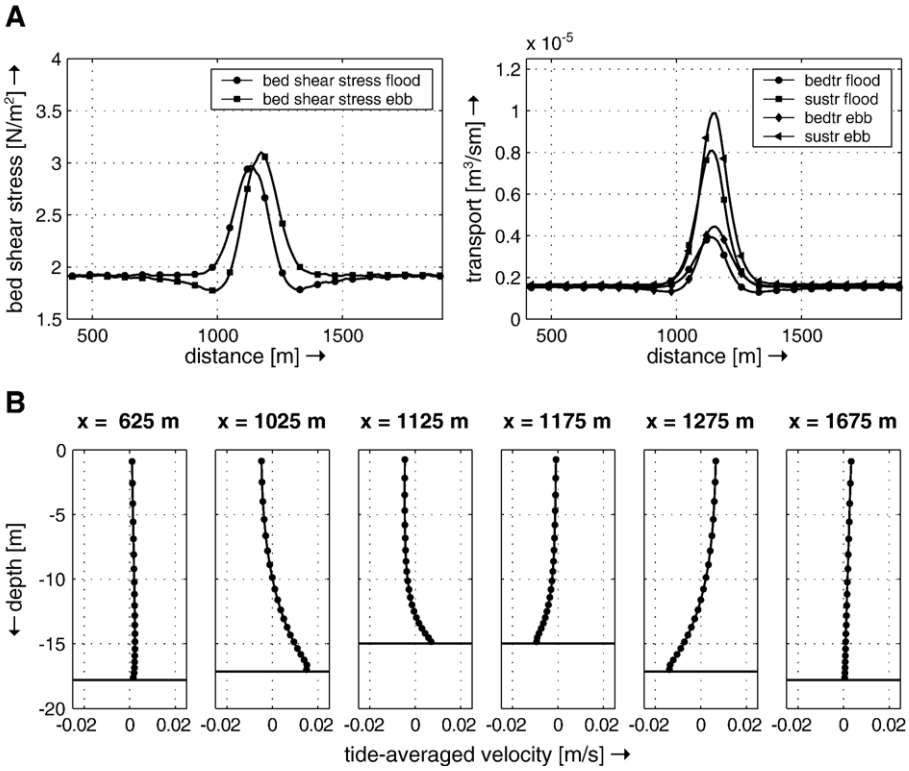

Fig. 7. A: Absolute bed-shear stress (left) and absolute bed-load and suspended-load transports (right) at maximum flood and maximum ebb (symmetrical tide) based on 2DV model simulation without waves. B: Tide-averaged velocity profiles at six locations for 2DV simulation without waves.

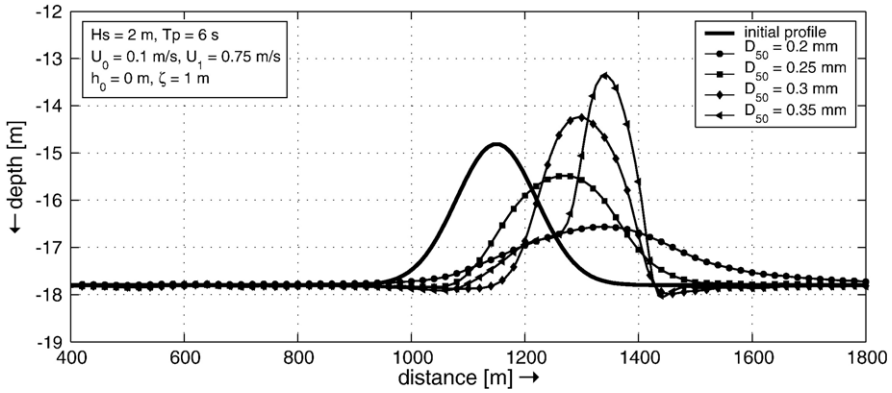

Fig. 8. Five-year bottom profile development for asymmetrical tide (net current of 0.1 m/s) with waves using a median sediment diameter (D_{50}) of 0.2,0.25, 0.3 and 0.35 mm.

in height using a median sediment diameter of 0.2 and 0.25 mm (dominant suspended load). The sand wave volume is about constant for sediment diameters in the range of 0.25 and 0.35 mm. The sand wave volume decreases considerably for very fine sand of 0.2 mm due to a relatively large contribution of the suspended-load transport. From these results it can be derived that the relative contributions of bed-load and suspended-load transports and the vertical distribution of the suspended transport determine the morphological development of the sand wave. Using coarser sediment particles, the bed-load transport and the suspended transport in the near-bed region are dominant and the sand wave increases in height due to the net transport effects toward the sand wave crest (circulation cell; see Fig. 3). Using finer sediment, the sand wave flattens due to the increased suspended-load transport by which particles are carried away from the crest region.

4.4.3. Effect of tides

Fig. 9 shows the five-year bottom profile development for simulations without waves using symmetrical tides with velocity amplitudes of 0.5, 0.75 and 1 m/s. It can be seen that the sand wave migrates in the southern (ebb) direction and increases in height. With increasing velocity amplitudes the sand wave height first increases as long as the bed-load transport is dominant. With a velocity amplitude of 1 m/s the suspended-load transport is dominant and the sediments are carried away from the crest region and the increase of the sand wave height with respect to the initial sand wave height is relatively small. From this figure it is found that when the suspended transport rate becomes dominant at a peak velocity of about 1 m/s, the sand wave remains approximately stable in height with an asymmetrical shape (steeper lee side flank).

4.4.4. Effect of bed roughness predictor

Fig. 10A shows the five-year bottom profile development from simulations with constant (C=65, 75 and 85 $m^{1/2}$/s) and variable bed roughness (due to ripples and megaripples) for the case of a velocity amplitude of 0.75 m/s and a net current of 0.1 m/s in flood direction with waves (H_s=2 m). It can be seen that the migration of the sand wave based on a variable bed roughness is reduced considerably. The roughness predictor generates a relatively large bed roughness during relatively low velocities and waves, assuming ripple-type bedforms to be present. The ripples are assumed to be washed out during relatively large velocities and wave heights, resulting in smaller transport rates and hence smaller migration rates.

Furthermore, a variable bed roughness yields a more symmetrical sand wave shape and a slightly larger sand wave height. A constant bed roughness leads to an asymmetrical (triangular) sand wave shape; the effect is largest for a roughness value of C=65 $m^{1/2}$/s. This small C-value (large roughness) results in larger bed-shear stresses (see Eq. (5a,b)) and

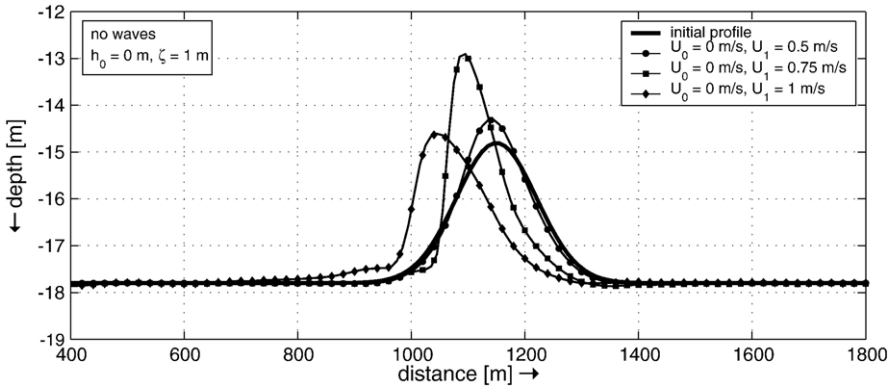

Fig. 9. Five-year bottom profile development in the case of symmetrical tide without a net current.

hence larger transport rates. Larger transport rates result in larger migration rates. Larger suspended-load transport also leads to reduction of the sand wave height. The bed-load and suspended-load transport rates at maximum flow of these runs are presented in Fig. 10B, showing larger transport rates for smaller *C*-values.

4.4.5. Effect of waves

Fig. 11A shows the five-year bottom profile development for simulations with a symmetrical tide for the case of a velocity amplitude of 0.75 m/s without a net current and with/without waves: H_s=0, 2 and 3 m. The wave direction is 315° to North and is taken to be constant in the spatial domain. It can be seen that the migration in southern ebb direction increases with increasing waves due to the increased wave stirring effect (especially during ebb with lower water depths and hence more effective stirring of sediments). The sand wave increases in height for simulations without waves and with moderate waves (H_s=2 m). In the case of relatively large waves (H_s=3 m) the sand wave decreases in height due to the relatively large bed-shear stresses at the sand wave crest; the sand wave volume increases in size due to the vertical circulation effects carrying sediment from the toe regions (scour holes) to the sand wave flanks which leads to a more asymmetrical development of the sand wave with a steeper south flank of the sand wave.

Fig. 11B shows bed-load and suspended-load transport rates at maximum flood and maximum ebb flow with waves (H_s=0, 2

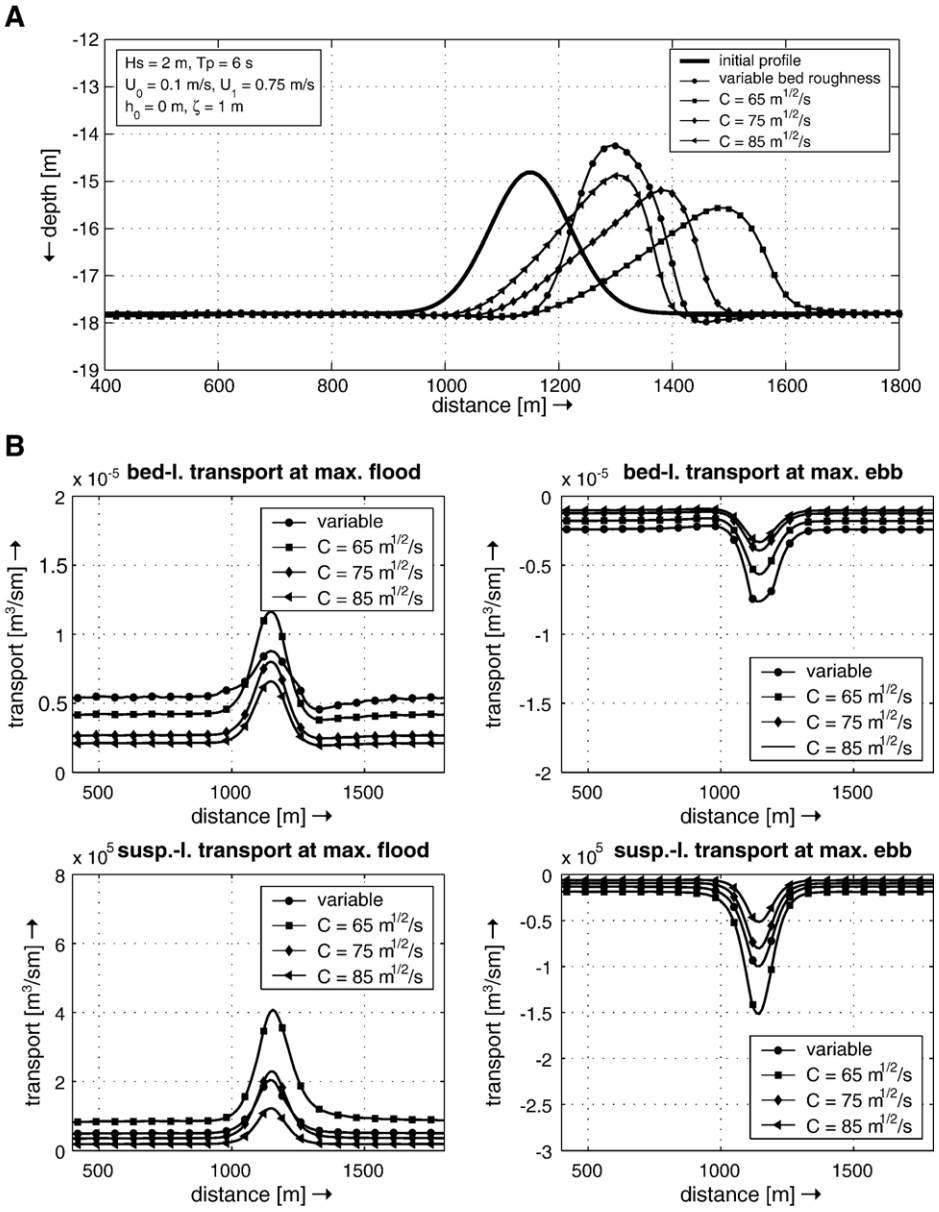

Fig. 10. A: Five-year bottom profile development in the case of asymmetrical tide with constant and variable bed roughness. B: Bed-load and suspended-load transport rates at maximum ebb and maximum flood with constant and variable bed roughness.

and 3 m) without a net current. It can be seen that bed-load and suspended-load transport rates during ebb are larger than during flood.

Fig. 12 shows the five-year bottom profile development for simulations for the case with a velocity amplitude of 0.75 m/s and a net current of 0.1 m/s (asymmetrical tide) in northern flood direction with waves: H_s=0, 2 and 3 m. It can be seen that without waves the sand wave development is strongly asymmetric after 5 years with the north flank being much steeper than the south flank. This case reflects the typical triangular-shaped dune migration in the lower flow regime as observed in unidirectional flow. When waves are superimposed, the transport rates during ebb flow are larger than those without waves and the sand wave migration is reduced. The south flank becomes steeper than the north flank and the sand wave crest shifts in southern (ebb) direction with increasing wave height (H_s=3 m), while the sand wave itself still migrates in northern (flood) direction due to the net current in flood direction.

4.4.6. Effect of longitudinal bed-slope factor

Fig. 13 shows the five-year bottom profile development in the case of an asymmetrical tide with waves based on simulations with different longitudinal bed-slope factors. This parameter which is based on the Bagnold approach (Bagnold, 1956) modifies the local bed-load transport on sloping beds by acting on the net bed-load transport over the wave cycle and thus influences the gross and net annual transport rates. This results in smaller bed-load transport rates in upsloping flow and larger values in downsloping flows resulting in the longitudinal spreading (smoothing) of the sand wave volume. Based on

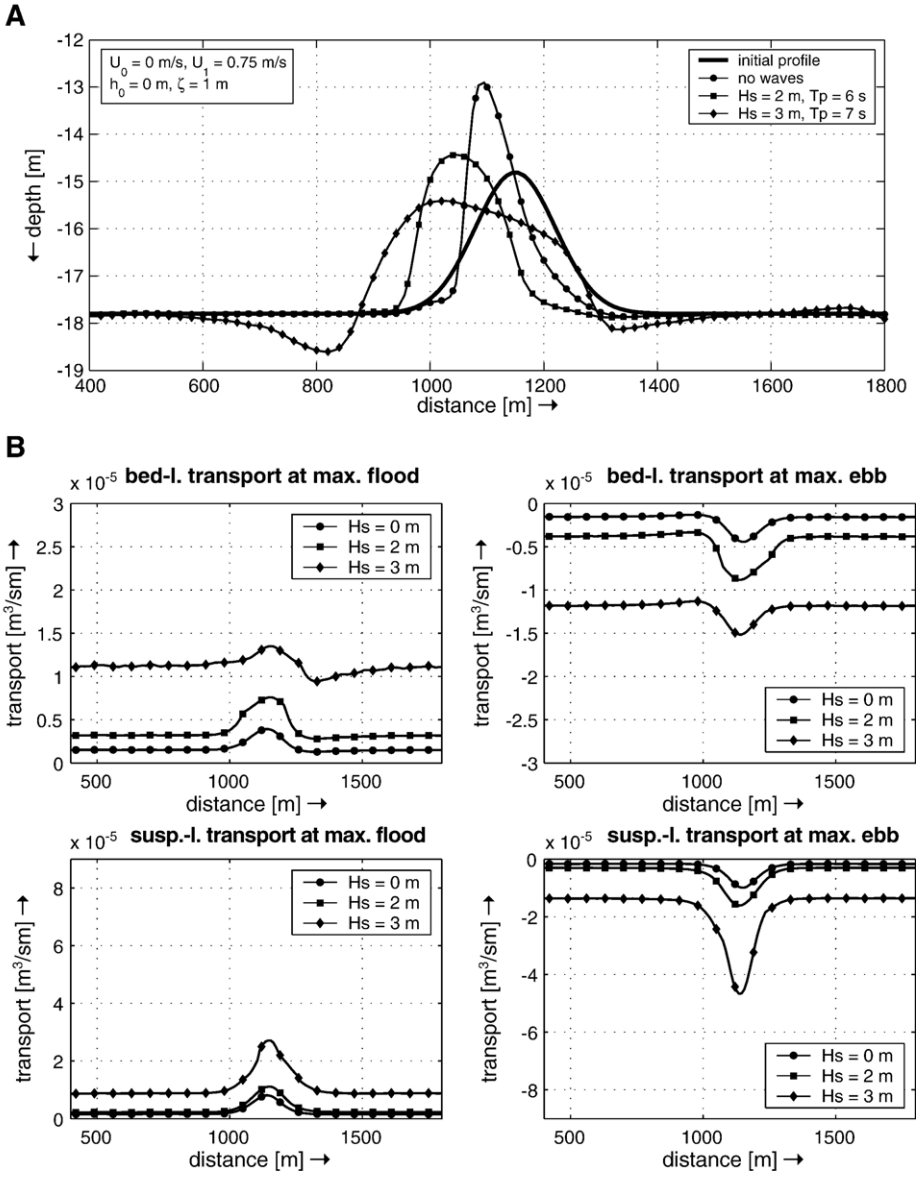

Fig. 11. A: Five-year bottom profile development in the case of symmetrical tide (U_0=0 m/s, U_1=0.75 m/s) with varying wave heights. B: Bed-load and suspended-load transport rates at maximum ebb and maximum flood with waves and no net current.

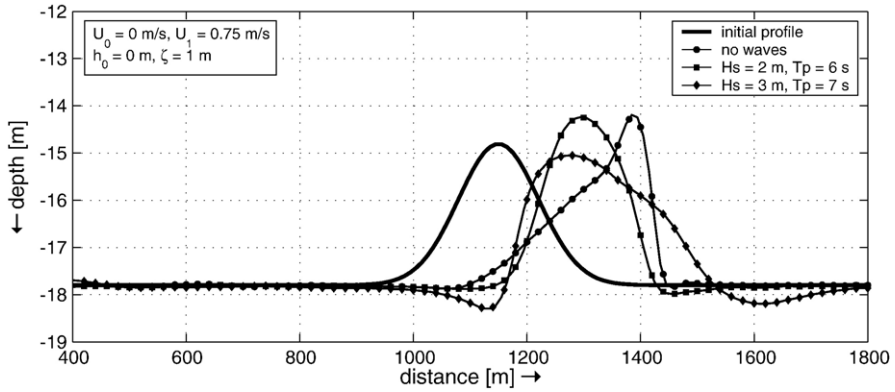

Fig. 12. Five-year bottom profile development in the case of asymmetrical tide (U_0=0.1 m/s, U_1=0.75 m/s) with varying wave heights.

analysis of experimental data on sloping beds, Van Rijn (1993, 2006a, submitted for publication) has shown that the Bagnold factor underpredicts the slope effects considerably in the lower transport regime. It may even be considered to apply the Bagnold factor to the reference concentration (boundary condition for suspended sediment concentrations) close to the bed. Experimental data (Smart, 1984) point to a larger effect in the case of graded sediments (wider size distribution). All these effects have been simulated by using a larger value in the range of 1 to 5 (default value is ALFABS=1), as shown in Fig. 13. Using longitudinal bed-slope factors (ALFABS) of 1, 3 and 5, it can be seen that the sand wave flattens. Larger values lead to flattening of the sand wave, as the bed-load transport in the upsloping flow region is reduced and increased in downsloping flow region. The sand wave volume remains the same. Numerical diffusion is negligibly small compared to the effect of the physical slope factor.

4.4.7. Synthesis of results for idealized sand wave

It has been shown that with a depth-averaged model approach the sand wave cannot increase in height as the modification of velocity profiles over the sand wave and hence the vertical circulation effects with net near-bed velocities along the flanks toward the sand wave crest (see Figs. 2 and 3) are not modelled. With a 2-dimensional vertical model approach this latter effect is properly taken into account, resulting in sand wave growth when bed-load transport is dominant. With increasing tidal velocities and wave heights the suspended-load transport becomes dominant and the sediments are carried away from the crest region to more outside locations from where they cannot be brought back to the crest in sufficient amount, resulting in a decrease of the sand wave height.

In the case of a symmetrical tide (no net current; U_1=0 m/s) the sand wave migrates in the southern (ebb) direction due to the dominant effect of the shallower water depth during ebb, which causes higher bed-shear stresses and hence transport rates in the ebb direction. The net migration direction (in southern or northern direction) of the sand wave is determined by the magnitude of the net current velocity and direction; in the case of a small net current in northern flood direction the sand wave migrates in the southern ebb direction due to the dominant effect of the shallower water depth during ebb. With increasing net current in northern flood direction, the effect of the shallower water is cancelled out and the sand wave migrates in northern flood direction.

Waves stir up sediments resulting in larger suspended-load transports and hence a reduction in height of the sand wave. Waves also affect the shape of the sand wave; with increasing waves the sand wave develops more asymmetrically. The effect of waves increases with diminishing water depth and therefore suspended transports during ebb (shallower water) increase more than suspended transports during flood. When waves are

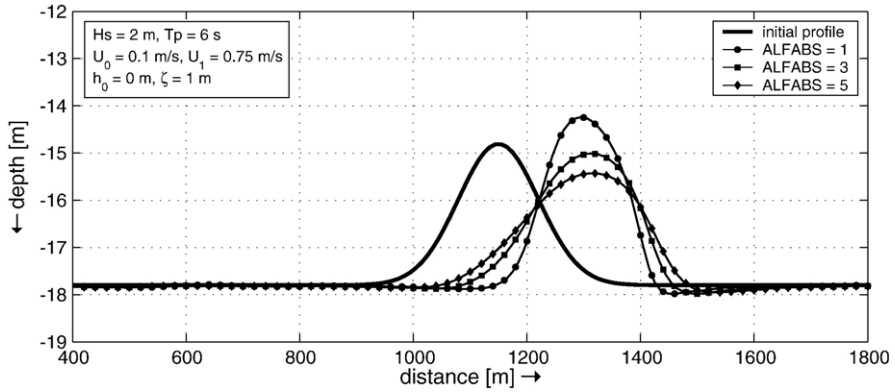

Fig. 13. Five-year bottom profile development in the case of asymmetrical tide with waves based on a longitudinal bed-slope factor (ALFABS) of 1, 3 and 5.

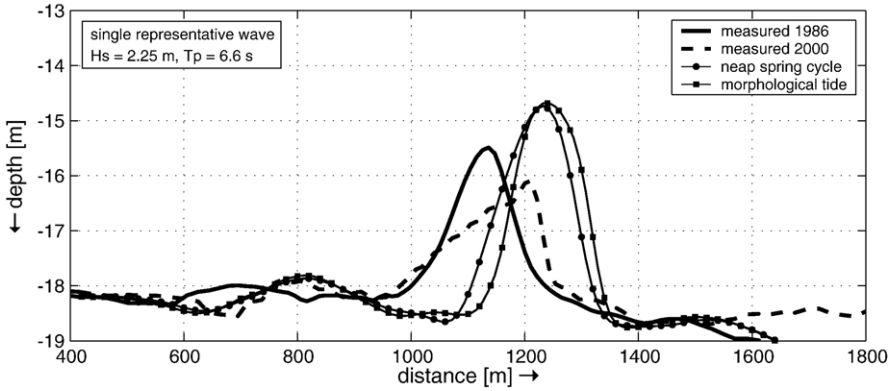

Fig. 14. Bottom profile development between 1986 and 2000 using a neap–spring tidal cycle and a morphological tide.

superimposed on a symmetrical tide (no net current), the sand wave migration is in the southern (ebb) direction. The sand wave migration changes to the northern flood direction, when waves are superimposed on a asymmetrical tide with a net northward current of 0.1 m/s due (dominant effect of net current).

The present conclusions are only valid for sand waves with heights of about 0.2 times the water depth and lengths of about 20 times the water depth and situated normal to the tidal velocity field. The effect of other length scales of the sand wave has not been studied, but it is most likely that the modification of the velocity profiles and the generation of recirculation cells will be different for very short sand waves and for very long sand waves.

5. Model runs for artificial sand wave at field site Hoek van Holland

This case refers to the 2DV simulation (cross-section 4, see Fig. 1A) of an artificial sand wave present in the North Sea (Hoek van Holland site). To reduce computational time, the neap–spring tidal velocity cycle with waves superimposed has been reduced to a representative (so-called morphological tide with one flood and ebb velocity cycle from the neap–spring cycle; see Fig. 1) producing a net annual transport rate of about 18 m^3/m/year in the (undisturbed) region south of the sand wave crest (at depth of about 18 m). The hydrodynamic boundary conditions were taken from the Holland coastal zone model (Roelvink et al., 2001). The schematisation is similar to that used in the 'idealized case' runs, except that now a realistic tidal curve is used, whereas the idealized case is based on a sinusoidal tidal curve. The particle size of the bed material is set to D_{50}=0.3 mm and D_{90}=0.6 mm. The wave spectrum at the sand wave location is represented by a single wave height of H_s=2.25 m with peak period of T_p=6 s, direction from west (315° to North) and a duration of 307 days per year based on the wave schematisation study of Walstra et al. (1997). The wave direction is assumed to be constant (315° to North) in the spatial domain of the sand wave. The combined wave and current action results in a net annual longshore transport of 18 m^3/m/year at a depth of about 18 m (ambient water depth), which is in line with earlier estimations (Van Rijn, 1997). Fig. 14 compares the bottom profile development of cross-section 4 between 1986 and 2000 from simulations using a neap–spring tidal cycle and the selected morphological tide. The sand volume of the original sand wave in cross-section 4 (between x=600 m and 1500 m with respect to −18.8 m depth level) is about 825 m^3/m based on the measured data of 1986, which reduces to about 805 m^3/m based on the measured data of 2000. These differences of about 3% may be caused by sounding errors. Computed and measured results are discussed in terms of quantitative parameters (sand wave dimensions, volume and migration speed) and qualitative aspects (sand wave shape; symmetry and asymmetry). As regards this latter aspect, the observations show a significant transition from a symmetric sand wave shape to an asymmetric shape over a period of 15 years. The maximum bed-slope is of the order of 1 to

Table 3
Model run input data and model results for field case sand wave near Hoek van Holland

Run	Tide	Waves	D_{50} (mm)	Bed roughness	Net annual transport (m^3/m /year)	Sand wave volume (m^3/m)
1	Neap–spring cycle	Single wave	0.3	Variable	18	882
2	Morphological tide	Single wave	0.3	Variable	18	882
3	Morphological tide	mv2-climate	0.3	Variable	24	917
4	Morphological tide	mv2-climate with storms	0.3	Variable	26	920
5	Morphological tide	Single wave	0.275	Variable	23	890
6	Morphological tide	Single wave	0.25	Variable	31	905
7	Morphological tide	Single wave	0.3	C = 65 $m^{0.5}$/s	22	905
8	Morphological tide	Single wave	0.3	C = 75 $m^{0.5}$/s	9	875
	Morphological tide	Single wave	0.3	C = 85 $m^{0.5}$/s	5	860
10	Morphological tide	Single wave	0.3	Variable without megaripples	11	883

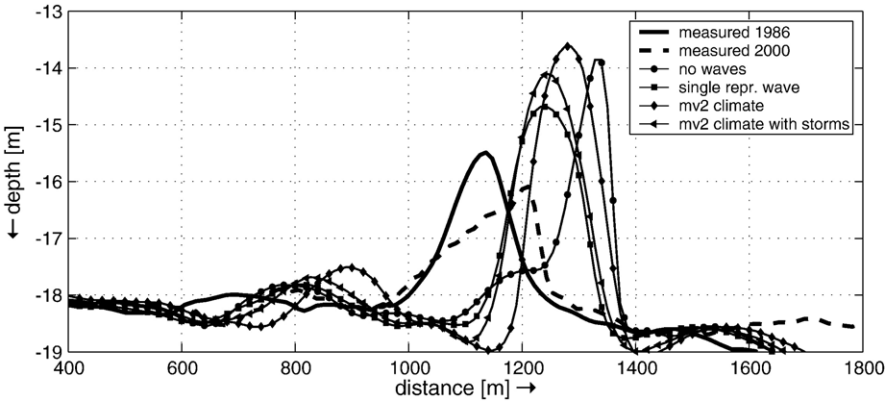

Fig. 15. Bottom profile development between 1986 and 2000 using different wave schematisations.

10 at the lee side (northern side). Hence, flow separation phenomena are not supposed to be of importance for this field case.

The computed migration of the sand wave is somewhat larger using the morphological tide, the height of the sand wave is approximately equal for both tidal schematisations. The sand volume increases to about 882 m^3/m (Fig. 14) based on computed results as sediment is trapped in the circulation cell. This computed increase of sand wave volume by about 8% is not observed from the bathymetry data.

Based on runs with the morphological tide over a period 1986 to 2000, the effect of variations in sediment diameter, different wave schematisations and various types of bed roughness on the bed evolution and sand wave volume has been studied. Basic input data and model results are given in Table 3. The net transport rates at the field site Hoek van Holland (Table 3) are somewhat smaller than those of the idealized case (Table 2), because the peak tidal current velocities at the real field site are somewhat smaller.

Morphological modelling of bed features in coastal seas requires the schematisation of the observed long-term wave spectrum into a set of wave classes, each with its representative wave height, wave period, wave direction and frequency of occurrence. Roelvink et al. (1998) have schematised the observed wave spectrum into 11 representative wave classes, which is referred to as the mv2-wave climate. The largest wave height of the mv2-climate is 2.75 m with a duration of 15.7 days per year. Extremely large storm waves were not separately taken into account, but included in the duration of the largest class. To obtain a more realistic schematisation with storm waves included, the highest wave condition of 2.75 m was replaced by 5 wave conditions varying from 2.75 to 5.0 m with a combined frequency of occurrence equal to that of the original wave condition. This latter schematisation is referred to as the mv2-climate with storms.

Fig. 15 shows the bottom profile development between 1986 and 2000 from simulations using different wave schematisations. It can be seen that without waves the sand wave migration is in northern (flood) direction and is larger than with waves. As the waves have more effect on sediment transport during ebb with smaller water depths, the sand wave migration is reduced. Using the mv2-climate, the sand wave increases in height compared to that of a single wave height, while the shape of the sand wave remains fairly symmetric. The mv2-climate with storms results in a smaller increase in sand wave height than that of the mv2-climate due to the inclusion of storm conditions flattening the sand wave. It is noted that the net annual sand transport (at depth of about 18 m) outside the sand wave region is modified using different wave schematisations. A single representative wave height yields a net annual transport of 18 m^3/m/year; the mv2-climate results in a value of 24 m^3/m/year and the mv2-climate with storms yields 26 m^3/m/year (30% increase with respect to that of a single representative wave; see Table 3). The sand volume of the sand wave increases slightly (see Table 3) with increased net annual transport, as more sediment is trapped in the circulation cell. Overall, it is concluded that the long-term

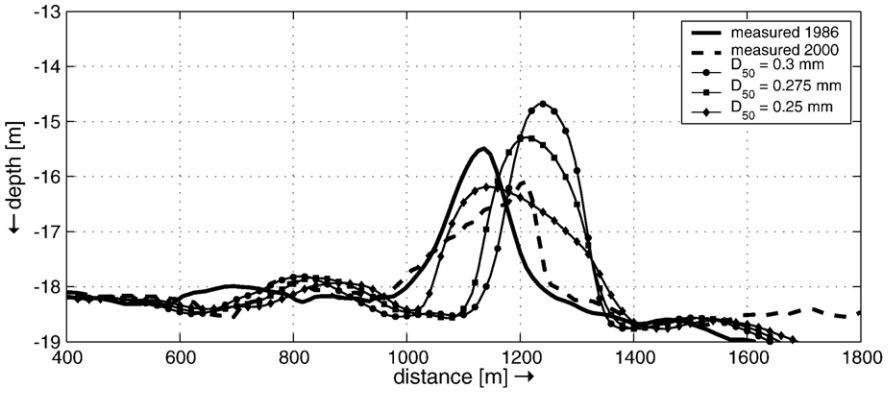

Fig. 16. Bottom profile development between 1986 and 2000 using a median sediment diameter (D_{50}) of 0.3, 0.275, and 0.25 mm.

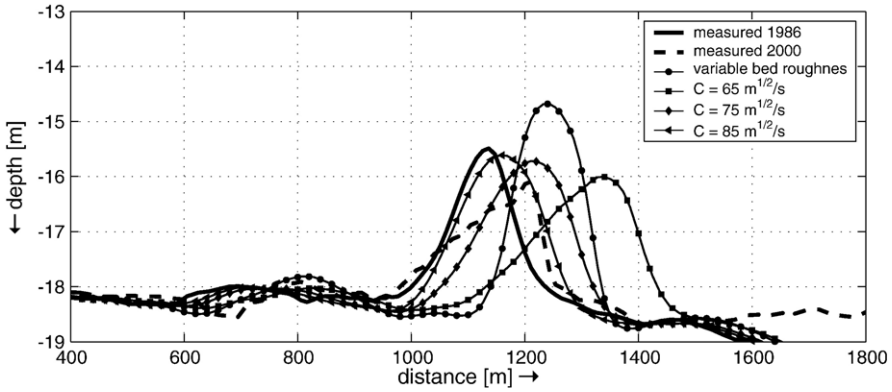

Fig. 17. Bottom profile development between 1986 and 2000 using variable and constant bed roughness.

morphological development of the sand wave can be simulated with reasonable accuracy using a single representative wave height (2.25 m) and direction.

The sediment diameter of the bed material varies in the range of 0.15 to 0.45 mm in the sand wave area. Generally, the bed material is somewhat coarser at the crest where wave action is largest and somewhat finer on the flanks of the sand wave. This variation in sediment diameter along the sand wave can only be represented by using a schematisation in multiple size classes (fractions), which is beyond the scope of the present study. Herein, only the effect of a different particle size (but constant along the sand wave) on the bed evolution is studied.

The sediment diameter affects the net annual transport rate and the ratio of bed-load and suspended-load transports and hence the morphological evolution. The sediment diameter has a significant effect on the value of the net annual sand transport (see Table 3): 18 m^3/m/year for D_{50}=0.3 mm (standard case), 23 m^3/m/year for D_{50}=0.275 mm and 31 m^3/m/year for D_{50}=0.25 mm. Fig. 16 shows the bed evolution between 1986 and 2000 for three different sediment diameters in the range of 0.25 to 0.3 mm. The sand wave volume increases from about 882 m^3/m for D_{50}=0.3 mm to 905 m^3/m for D_{50}=0.25 mm (for decreasing sediment diameter), see Table 3. Slightly more sediment is trapped in the circulation cell for finer sediment. Overall, the computations using finer sediment lead to an increase of the sand wave volume of about 8% to 10% (after 15 years) with respect to the original volume of 825 m^3/m due to trapping of sediment in the circulation cell. A smaller sediment diameter also leads to a relatively large contribution of suspended-load transport resulting in flattening of the sand wave, whereas a larger sediment diameter results in a larger bed-load transport contribution and hence an increase of the sand wave height and larger migration to the north.

Fig. 17 shows the bed profile development for simulations with constant (C=65, 75 and 85 $m^{1/2}$/s) and variable bed roughness (roughness predictor). It can be seen that a variable roughness (which includes ripple and megaripple roughness effects) yields a more symmetrical sand wave shape and a larger sand wave height. A relatively small, constant bed roughness of C=65 $m^{0.5}$/s leads to an asymmetrical (triangular) sand wave shape and a relatively large migration rate. A small C-value (C=65 $m^{0.5}$/s) results in relatively large bed-shear stresses (see Eq. (5a,b)) and hence larger suspended transport rates (more turbulence) leading to a larger migration rate and a reduction of the sand wave height. The sand wave becomes asymmetric (in agreement with the observed bed profile) for a small C-value of 65 $m^{0.5}$/s, but the migration speed is much too large. The bed roughness has a strong effect on the net annual transport (see Table 3). The smallest C-value (rougher bed) results in the largest bed-shear stresses and hence a relatively large transport rate of 22 m^3/m/year. The net annual transport is reduced to the range of 5 to 10 m^3/m/year for C in the range of 85 to 75 $m^{0.5}$/s. Rather good agreement between predicted and measured bed profiles (Fig. 17) can be observed for these C-values. Finally, a

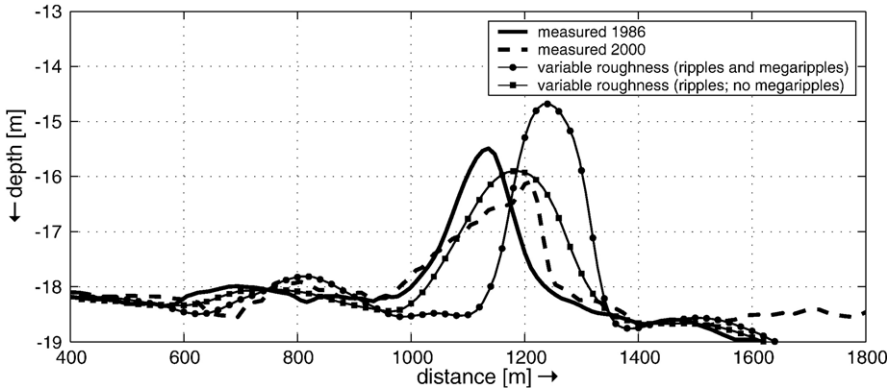

Fig. 18. Bottom profile development between 1986 and 2000 using variable bed roughness (predictor) with and without megaripple roughness.

run was done using a variable bed roughness without the effect of megaripples (this latter effect is optional for the model user). This assumption (no megaripple roughness effect) leads to larger C-values in the range of 75 to 85 $m^{0.5}/s$ (smoother bed) and smaller bed-shear stresses and hence a smaller net annual transport rate of about 11 $m^3/m/year$ (see Table 3). Fig. 18 shows very good agreement between the measured and computed bed evolution after 15 years. These C-values of 75 to 85 $m^{0.5}/s$ for a depth of 18 to 20 m result in k_s-values in the range of 0.005 to 0.015 m (small-scale ripples; almost flat bed). The combination of parameters of Run 10 (Fig. 18) produces the best overall results in terms of sand wave dimensions, volume and migration speed compared to the measured data, but the computed sand wave shape is too symmetric.

These results suggest that the net annual transport rate of 18 $m^3/m/year$ used in earlier studies (Van Rijn, 1997) may be somewhat too large for this particular location with an artificial sand wave in the neighbourhood of a dumping site for muddy materials. The model results also suggest the presence of a rather smooth bed without the existence of larger-scale megaripples. Analysis of detailed level soundings (Van Woudenberg, 1996) shows the presence of megaripples at the south flank of the sand wave. Van Dijk and Kleinhans (2005) have observed that megaripples migrating over sand waves are common features in the North Sea, but they have also observed seasonal variations in the presence of megaripples, depending on the occurrence of storms. Megaripples tend to be washed out during stormy seasons. It is clear that these effects are insufficiently taken into account by the new bed roughness predictor. The model results suggest that the megaripples are insufficiently washed out during storms.

6. Conclusions

This paper has studied the morphological behaviour of an artificial sand wave normal to the tidal currents at the Dutch shoreface near Rotterdam harbour (water depths in the range of 15 to 20 m). The sand wave was made in the period 1982 and 1986 by dumping 3.5 Mm^3 sand. Between 1986 and 2000 the sand wave migrated to the north (in the dominant flood direction) over a distance of about 100 m. The DELFT3D model was used to simulate the observed morphological behaviour of the sand wave. This model was also used to study the morphological behaviour of an idealized sand wave to gain insight of the physical processes at the sand wave and to study the effect of tides, waves and basic model settings. The main findings of the study can be summarized in the following conclusions:

- the artificial sand wave with a height of 3 to 4 m has survived over a period of 15 years and slowly migrates in northern direction (dominant flood direction) with slightly reduced height;
- the basic cause of sand wave growth is the deformation of the velocity profiles along the sand wave morphology resulting in a vertical circulation cell with net (time-averaged) velocities toward the sand wave crest in the near-bed region; in the case of dominant bed-load transport this results in a constant flow of sediments to the sand wave crest; the effect of sand wave growth can only be represented by using a 3D model resolving the vertical structure of the flow;
- the model results show that the sand wave grows in the case of dominant bed-load transport (weak tidal currents; relatively coarse sediment; small roughness height; low waves) and that the sand wave decays in the case of dominant suspended transport (strong currents, relatively fine sediment, large roughness height; storm waves);
- the model results show that a sand wave migrates in the ebb direction in the case of a symmetrical tide (no net current) due to larger bed-shear stress during ebb flow with smaller water depths; this effect can only be modelled if the Chézy coefficient is allowed to vary in the computational domain;
- the migration direction changes from the ebb direction to the flood direction when a dominant current in the flood direction is added to the symmetrical tidal motion;
- when waves (with constant direction and approximately normal to the coast and the tidal velocity field) are superimposed on the tidal current, the effect is largest during ebb flow with smaller water depths; waves enhance the migration of the sand wave in the ebb direction; waves also lead to a reduction of the sand wave crest height by stirring more sediments from the crest into suspension which are carried away by the tidal currents from the sand wave crest where wave action is largest; the morphological development is simulated with reasonable accuracy using a single representative wave height and direction;
- the bed roughness has a dominant effect on the ratio of bed-load and suspended-load transports, on the net annual transport rate and on the migration rate of the sand wave; the bed evolution after 15 years can be very well represented by using a variable bed roughness (based on a predictor) neglecting the effect of megaripples resulting in C-values of about 80 $m^{0.5}/s$.
- the computed results show that the sand wave dimensions, volume and migration speed can be represented reasonably well, but the computed sand wave shape generally is too symmetric.

The present conclusions are only valid for sand waves with heights of about 0.2 times the water depth and lengths of about 20 times the water depth and situated normal to the tidal velocity field. The effect of other length scales of the sand wave has not been studied, but it is most likely that the modification of the velocity profiles and the generation of recirculation cells will be different for very short sand waves and for very long sand waves.

The applied 2DV approach seems to be valid for the present field case near Hoek van Holland, since the tidal flow is parallel to the coast and the sand wave crest is normal to the coast. Oblique flow does not occur and wave-induced cross-shore transport processes are negligibly small (Van Rijn, 1997) at these relatively large water depths (about 15 to 20 m). Finally, it is noted that the present results are only valid for the shoreface with water depths in the range of 15 to 20 m. It is uncertain whether these conclusions can be extrapolated to more offshore

locations with much larger water depths, where the transport rates are much smaller (limited effect of waves) and net transport rates are difficult to define. It is unlikely that the present approach can be used to determine the final long-term equilibrium shape of the sand waves (if existing?). This requires a computational effort on the time scale of centuries, which is not feasible at present computer power. However, the measured and computed results show that artificially created tidal sand waves can survive over very long time scales (decades) in deeper water with depths of about 20 m, where the effect of waves is relatively small. Both the measured and model results show that the artificial sand wave at a site with an originally flat bed will eventually decay (about 15% decay in height over 15 years). The time scale of decay at this site will be very much dependent on the magnitude and frequency of future storm events, and is intuitively estimated to be in the range of 50 to 100 years.

Future research will be focussed on sand waves oblique to the tidal current, the dimensions of the sand waves (different length and height scales) and the schematisation of the bed material into multiple size fractions, so that the particle sorting effects (coarser sediment on the crest) can be better simulated. Additional field measurements are required to study the distribution of the bed material composition (box cores) along the sand wave and the presence of bedforms (small-scale or large-scale ripples) in relation to the proper bed roughness.

Acknowledgements

The Directorate Noordzee (North Sea) and the National Institute of Coastal and Marine Management (RIKZ) of Rijkswaterstaat are both gratefully acknowledged for providing bathymetry data of the sand wave near Hoek van Holland, The Netherlands.

References

Bagnold, R.A., 1956. The flow of cohesionless grains in fluids. Proc. Royal Soc. Philos. Trans., London, vol. 249, pp. 71–81.

Besio, G., Blondeaux, P., Frisina, P., 2003. A note on tidally generated sand waves. Journal Fluid Mechanics 485, 171–190.

Besio, G., Blondeaux, P., Brocchini, M., Vittori, G., 2004a. On the modelling of sand wave migration. Journal of Geophysical Research 109 (C4), 1–13 C04018.

Besio, G., Blondeaux, P., Vittori, G., 2004b. Teoria unificata per lo studio della formazione di sand waves e sand banks. Proceedings XXIX Convegno di Idraulica e Costruzioni Idrauliche, Trento, 7–10 September, vol. 3, pp. 689–696.

Galappatti, R., 1983. A Depth-Integrated Model for Suspended Transport. Report No. 83–7. Delft University of Technology, Delft, The Netherlands.

Ikeda, S., 1982. Lateral Bed-Load Transport on Side Slopes. Journal Hydraulics Division, ASCE 108 (11).

Hulscher, S., 1996a. Formation and migration of large-scale, rhythmic sea-bed patterns: a stability approach. Doctoral Thesis, Department of Oceanography, University of Utrecht, The Netherlands.

Hulscher, S., 1996b. Tidal-induced large-scale regular bed form patterns in a three-dimensional shallow water model. Journal of Geophysical Research 101 (C9), 20727–20744.

Hulscher, S.J.M.H., De Swart, H.E., de Vriend, H.J., 1993. The generation of offshore tidal sand banks and sand waves. Continental Shelf Research 13 (11), 1183–1204.

Huthnance, J., 1982. On one mechanism forming linear sand banks. Estuarine, Coastal and Shelf Science 4, 79–99.

Lesser, G., Roelvink, J.A., Van Kester, J.A.T.M., Stelling, G.S., 2004. Development and validation of a three-dimensional morphological model. Journal of Coastal Engineering 51, 883–915.

Meene, J.W.H., 1994. The shoreface-connected ridges along the central Dutch coast. Doctoral Thesis, Department of Physical Geography, University of Utrecht, The Netherlands.

Nemeth, A.A., Hulscher, S.J.M.H., DeVriend, H.J., 2002. Modelling sand wave migration in shallow shelf seas. Continental Shelf Research 22 (18–19), 2795–2806.

Roelvink, J.A., VanHolland, G., Bosboom, J., 1998. Morphological study MV2, Phase 1. Validation morphological modelling Haringvliet entrance (in Dutch). WL | Delft Hydraulics, Report Z2428. Delft, The Netherlands.

Roelvink, J.A., Van der Kaaij, T., Ruessink, B.G., 2001. Calibration and verification of large-scale 2D/3D flow models. Phase 1, Parcel 2, Subproduct 2, ONL FLYLAND report. WL | Delft Hydraulics report Z3029.11. Delft, The Netherlands.

Roos, P.C., 2004. Seabed pattern dynamics and offshore sand extraction. Doctoral Thesis, Dep. of Civil Engineering, University of Twente, The Netherlands.

Roos, P.C., Hulscher, S.J.M.H., Knaapen, M.A.F., Van Damme, R.M.J., 2004. The cross-sectional shape of tidal sandbanks: Modeling and observations. Journal of Geophysical Research 109, F02003. doi:10.1029/2003JF000070.

Smart, G.M., 1984. Sediment transport formula for steep channels. Journal of Hydraulic Engineering 110 (3), 267–276.

Van Dijk, T.A.G.P., Kleinhans, M.G., 2005. Processes controlling the dynamics of compound sand waves in the North Sea, Netherlands. Journal of Geophysical Research 110, F04S10.

Van Rijn, L.C., 1984. Sediment transport, Part II: Suspended load transport. Journal of Hydraulic Engineering, ASCE 110 (10).

Van Rijn, L.C., 1993. Principles of sediment transport in rivers, estuaries and coastal seas. Aqua Publications, The Netherlands. (www.aquapublications.nl).

Van Rijn, L.C., 1997. Sediment transport and budget of the central coastal zone of Holland. Coastal Engineering 32, 61–90.

Van Rijn, L.C., 2006a. Principles of sediment transport in rivers, estuaries and coastal seas (update 2006). Aqua Publications, The Netherlands. (www.aquapublications.nl).

Van Rijn, L.C., submitted for publication. A unified view of sediment transport by currents and waves, Part I, II, III and IV, Journal of Hydraulic Engineering.

Van Rijn, L.C., Walstra, D.J.R., Van Ormondt, M., 2004. Description of TRANSPOR2004 and implementation in DELFT3D-ONLINE: final report. WL | Delft Hydraulics report Z3748.10. Delft, The Netherlands.

Van Woudenberg, C.C., 1996. Artificial sand wave at location Hoek van Holland (in Dutch). MSc Thesis/Report NZ-96–03, Dir. Noordzee, The Hague, The Netherlands.

Vittori, G., Blondeaux, P., Hulscher, S.J.M.H., Piqueret, M., Roos, P.C., 2005. Potential use of sand waves and sand banks for sand mining, Paper K. In: Van Rijn, et al. (Ed.), Sandpit, sand transport and morphology of offshore sand mining pits. Aqua Publications, The Netherlands (www.aquapublications.nl).

Walstra, D.J.R., Reniers, A.J.H.M., Roelvink, J.A., Wang, Z.B., Steetzel, H.J., Aarninkhof, S.G.J., Van Holland, G., Stive, M.J.F., 1997. Morphological impact of large-scale marine sand extraction (in Dutch). WL | Delft Hydraulics report Z2255. Delft, The Netherlands.